

HST and ground-based eclipse observations of V2051 Ophiuchi: Binary parameters[★].

Raymundo Baptista¹, M. S. Catalán², Keith Horne³ and D. Zilli¹

¹ *Departamento de Física, Universidade Federal de Santa Catarina, Campus Trindade, 88040-900, Florianópolis - SC, Brazil, email: bap@fsc.ufsc.br, zilli@fsc.ufsc.br*

² *Department of Physics, Keele University, Keele, Staffordshire, ST5 5BG, UK, email: msc@astro.keele.ac.uk*

³ *School of Physics & Astronomy, University of St. Andrews, North Haugh, St. Andrews, Fife, KY16 9SS, Scotland, email: kdh1@st-and.ac.uk*

Accepted 199? July ?. Received 199? June ?; in original form 1998 January 5

ABSTRACT

We report on high-speed eclipse photometry of the dwarf nova V2051 Oph while it was in a low brightness state, at $B \simeq 16.2$ mag. In comparison to the average IUE spectra, the ultraviolet continuum and emission lines appear reduced by factors of, respectively, $\simeq 4$ and $\simeq 5$. Flickering activity is mostly suppressed and the lightcurve shows the eclipse of a compact white dwarf at disc centre which contributes $\simeq 60$ per cent of the total light at 3900–4300 Å.

We use measurements of contact phases in the eclipse lightcurve to derive the binary geometry and to estimate masses and relevant dimensions. We find a mass ratio of $q = 0.19 \pm 0.03$ and an inclination of $i = 83 \pm 2$ degrees. The masses of the component stars are $M_1 = 0.78 \pm 0.06 M_\odot$ and $M_2 = 0.15 \pm 0.03 M_\odot$. Our photometric model predicts $K_1 = 83 \pm 12 \text{ km s}^{-1}$ and $K_2 = 435 \pm 11 \text{ km s}^{-1}$. The predicted value of K_1 is in accordance with the velocity amplitude obtained from the emission lines after a correction for asymmetric line emission in the disc is made (Watts et al. 1986).

The secondary of V2051 Oph is significantly more massive than the secondaries of the other ultra-short period dwarf novae. V2051 Oph is probably a relatively young system, whose secondary star had not enough time to evolve out of thermal equilibrium. A consequence would be that V2051 Oph has a lower mass transfer rate than the other ultra-short period dwarf nova. This would explain why outbursts in V2051 Oph are so rare.

Key words: binaries: close – novae, cataclysmic variables – eclipses – stars: individual: (V2051 Ophiuchi).

1 INTRODUCTION

Cataclysmic Variables (CVs) are close binary systems in which mass transfer occurs from a late-type star filling its Roche lobe to a companion white dwarf via an accretion disc or column (Warner 1996). The subclass of the dwarf novae comprises systems in which the white dwarf is non-magnetic ($B \lesssim 10^4$ G) and which are mostly known for their recurrent, large amplitude outbursts ($\Delta m = 3 - 5$ mag,

typical duration of 5-10 days). These outbursts reflect a change in the structure of their discs – from a cool, optically thin, low viscosity state to a hot, optically thick, high viscosity state – and which are usually parameterized as a large change in the mass accretion rate ($\dot{M} = 10^{-11} M_\odot \text{ yr}^{-1} \mapsto 10^{-9} M_\odot \text{ yr}^{-1}$. See, e.g. Pringle, Verbunt & Wade 1986). In quiescence, when the accretion disc is faint, the white dwarf and the bright spot (where the stream of transferred matter hits the edge of the accretion disc) dominate the optical and ultraviolet light from the system, and can be seen as sharp changes in the slope of the lightcurve in eclipsing systems. From the timings of these features, a precise determination of the binary parameters can be obtained.

V2051 Oph is an eclipsing dwarf nova with an orbital period of 90 minutes. High speed photometry by Warner (1983) and Cook & Brunt (1983) shows that the orbital

[★] Based on observations with the NASA/ESA *Hubble Space Telescope*, obtained at the Space Telescope Science Institute, which is operated by the Association of Universities for Research in Astronomy, Inc., under NASA contract NAS 5-2655, and on observations made at Laboratório Nacional de Astrofísica/CNPq, Brazil.

lightcurve is characterized by deep eclipses ($\Delta B \simeq 2.5$ mag) and large amplitude flickering ($\gtrsim 30$ per cent), responsible for a variety of eclipse morphologies. Significant (> 50 per cent) brightness changes occur on timescales shorter than the orbital period but no stable orbital hump (associated to anisotropic emission from a bright spot) precedes the eclipse. Unlike most dwarf novae, which usually display an orbital hump with maximum at phase ~ 0.8 , in V2051 Oph the humps apparently occur at any orbital phase (Berriman, Kenyon & Bailey 1986). The compact source usually seen at disc centre is variable both in brightness and in the duration of its immersion and emergence (from $\simeq 50$ to 80 s), and was interpreted by Warner & Cropper (1983) to be the inner region of the disc and not the white dwarf. Only one relatively short outburst of V2051 Oph has been reported since its discovery, in which it reached $B \simeq 13$ mag (Warner & O’Donoghue 1987). The analysis of optical and infrared lightcurves led Berriman et al. (1986) to suggest that the accretion disc in V2051 Oph consists largely of optically thin material, in accordance with the observed color changes during eclipse (Cook & Brunt 1983). V2051 Oph was proposed to be a low field polar system by Warner & O’Donoghue (1987) – a possibility first mentioned by Bond & Wagner (1977) – based on the interpretation of their eclipse maps and on the observation of a 42 s oscillation in the optical during outburst, reminiscent of the rapid oscillations seen in polars. However, in quiescence the emission lines are double peaked and exhibit the classical rotational disturbance effect during eclipse, suggesting the existence of a prograde accretion disc (Cook & Brunt 1983; Watts et al. 1986). Watts et al. (1986) combined the measured K_1 value with velocity-dependent eclipse data of the emission lines to derive a dynamical solution for the binary, obtaining $M_1 = 0.43 M_\odot$, $M_2 = 0.11 M_\odot$ and a radius $R_2 = 0.15 R_\odot$. They also fit the ultraviolet to optical spectrum with a steady-state optically thick disc model to find $\dot{M} = 1.3 \times 10^{-10} M_\odot \text{ yr}^{-1}$ and a distance to the system between 90 and 150 pc.

V2051 Oph belongs to a small group of ultra-short period eclipsing dwarf nova together with Z Cha, OY Car and HT Cas. Binary parameters for those other systems have been determined with high precision using the method described by Cook & Warner (1984) to derive the mass ratio, inclination and white dwarf radius from the white dwarf and bright spot eclipse phases. In V2051 Oph, the absence of a well defined bright spot and the uncertainty in associating the compact central source with the white dwarf (due to its variability both in width and brightness) has, until now, precluded the use of this method to derive its binary parameters.

In this paper we present and discuss Hubble Space Telescope and ground-based eclipse observations while V2051 Oph was in an occasional low brightness state. The data are described in section 2. In section 3 we use contact phases of the white dwarf and bright spot to develop a purely photometric model for the binary, deriving masses and radii of both stars, the binary inclination and the orbital separation. Section 4 discusses possible systematic effects affecting the derived binary parameters, possible causes for the observed low brightness, the secondary star and the evolutionary stage of V2051 Oph. Our results are summarized in section 5.

2 OBSERVATIONS

2.1 HST/FOS high-speed spectroscopy

The *Faint Object Spectrograph* (FOS) onboard the *Hubble Space Telescope* (HST) was used to obtain time-resolved spectroscopy of two consecutive eclipses of the dwarf nova V2051 Oph on 1996 January 29. The observations, summarized in Table 1, consist of two series of exposures in the RAPID readout mode at a time resolution of 3.38 s and a dead-time between exposures of 0.1 s. During data acquisition, the spectrum was shifted electronically by 1/2 of a diode along the 516 diode Digicon array (‘1/2 sub-stepping’) resulting in a 1032-pixel spectrum with a net exposure time of $1.64 \text{ s pixel}^{-1}$. The first run (H1) was carried out using a $0.86''$ circular aperture and the G400H grating (spectral resolution $\Delta\lambda = 1.5 \text{ \AA pixel}^{-1}$) and covered the egress of the first eclipse. The second run (H2) was performed using a $0.86'' \times 0.86''$ square aperture and the G160L grating ($\Delta\lambda = 3.5 \text{ \AA pixel}^{-1}$) and covered the following eclipse. The spectral range covered by the HST observations is, respectively for the G160L and the G400H data, 1150 – 2500 Å and 3200 – 4800 Å.

The observations were reduced using procedures similar to the standard STSDAS pipeline, and included flat-field and geomagnetically induced motion (‘GIMP’) corrections, background and scattered light subtraction, wavelength and absolute flux calibrations. The absolute photometric accuracy of these observations should be about 4 per cent.

For the G160L observations, the undispersed order-zero light is also recorded on the diode array, providing a broadband UV-optical photometric measurement that is simultaneous with each of the ultraviolet spectra. The order-zero light has a passband with a FWHM of 1900 Å and a pivot wavelength of 3400 Å. To convert counts to flux densities we used the predicted post-COSTAR response of $950 \text{ counts s}^{-1} \text{ mJy}^{-1}$ of Eracleous & Horne (1994), which has an uncertainty of 50 per cent.

Average out-of-eclipse and mid-eclipse spectra of the G160L data are shown in the upper panel of Fig. 1. The most prominent lines and bands are labeled. The comparison of the G160L out-of-eclipse spectrum with the average IUE spectrum of Watts et al. (1986) reveals that V2051 Oph was considerably fainter than usual at the time of the HST observations. The flux in the continuum and the emission lines have been reduced by factors of, respectively, $\simeq 4$ and $\simeq 5$. The lower panel of Fig 1 shows average out-of-eclipse and mid-eclipse spectra of the G400H data. The G160L order-zero passband overlaps the spectral coverage of the G400H data. Filled squares show the fluxes of the G160L order zero light computed at the same orbital phase ranges as the G400H average spectra. This comparison indicates that V2051 Oph remained at roughly the same brightness level during the HST observations.

Lightcurves at selected passbands for both HST runs are shown in Fig. 2. These will be discussed in detail in section 2.4.

2.2 high-speed photometry

High-speed photometry of V2051 Oph was obtained with the 1.6 m telescope of Laboratório Nacional de Astrofísica

Table 1. Journal of the observations.

date (1996)	run	Start (UT)	Δt (s)	No. of exposures	Spectral range	Phase range (cycles)	Instrument
Jan 29	H1	19:03	3.38	113	3226-4781 Å	+0.01, +0.08	HST/FOS/BL
Jan 29	H2	20:24	3.38	693	1150-2507 Å	-0.09, +0.34	HST/FOS/BL
Jun 15	L1	22:21	5.0	547	B-band	-0.24, +0.27	FOTRAP
Jun 16	L2	22:24	5.0	398	white light	-0.18, +0.18	FOTRAP
Jun 16	L3	23:45	5.0	516	white light	-0.29, +0.19	FOTRAP
Jun 17	L4	22:19	5.0	432	white light	-0.23, +0.17	FOTRAP

(LNA/CNPq), in southern Brazil, on 1996 June 15-17. Four eclipses were collected, one in the B-band and the remaining in white light (W). These observations are detailed in Table 1.

The observations were performed with the one-channel FOTRAP photometer in its single-filter mode at a time resolution of 5 s, using a 11.3" diaphragm. A Hamamatsu R943-02 PMT was employed. Sky measurements were taken at intervals of 15-20 min at a position 20" to the north of the variable, except during eclipse. The sky measurements were fitted by a low-order polynomial and then subtracted from the raw data. A close comparison star was also regularly observed to check for the presence of clouds and sky transparency variations. From these observations, we confirmed that all 4 runs were performed under good sky conditions. Coefficients of extinction and of transformation to the UBVR standard system were derived from observations of E-region stars of Graham (1982) and blue spectrophotometric standards of Stone & Baldwin (1983). The reader is referred to Jablonski et al. (1994) for a detailed study of the reliability of the transformations from FOTRAP's natural to the standard UBVR system, in particular for objects of peculiar spectra such as CVs. We used the relation of Lamla (1981), $B = 2.5 \log f_B(\text{mJy}) - 16.57$, to transform B magnitudes to flux density units. The absolute calibration of the B-band observations is accurate to better than 4 per cent.

The ground-based lightcurves of V2051 Oph are shown in Fig. 3 and will be discussed in section 2.4.

2.3 New eclipse timings

Mid-eclipse times of V2051 Oph were measured by employing the bisected chord method and by computing the midpoint of the phases of maximum and minimum derivative in the lightcurves (section 3). These methods yield values which are consistent with each other under the uncertainties, and therefore we adopted the mean as the mid-eclipse time. The new heliocentric (HJD) as well as barycentric (BJED) timings of V2051 Oph are listed in Table 2 with corresponding cycle number and uncertainties (quoted in parenthesis). Also shown are the (O-C) values with respect to the revised linear ephemeris of Baptista, Triplet & Bond (1998),

$$T_{mid} = \text{BJED } 2\,443\,245.977\,850 + 0.062\,427\,8595 \times E \quad (1)$$

The measured (O-C) values are in accordance with the cyclical variations in the orbital period of V2051 Oph observed by Baptista, Triplet & Bond (1998).

Table 2. New eclipse timings.

Cycle	HJD (2,450,000+)	BJED (2,450,000+)	(O-C) ^a (cycles)
109988	112.29277	112.29273(4)	-0.0084
109989	112.35517	112.35513(4)	-0.0089
112201	250.44558	250.44555(2)	-0.0090
112217	251.44443	251.44440(1)	-0.0089
112218	251.50688	251.50685(1)	-0.0086
112233	252.44331	252.44328(2)	-0.0084

^a Observed minus calculated times with respect to the ephemeris of eq.1.

2.4 Eclipse lightcurves

We adopted the following convention regarding the phases: conjunction occurs at phase zero, the phases are negative before conjunction and positive afterwards. The lightcurves were phased according to the linear ephemeris of eq. 1. A phase correction of +0.0087 cycles was further applied to the data to make the centre of the white dwarf eclipse coincident with phase zero (see section 3).

V2051 Oph was particularly faint at the time of both the HST and the ground-based observations. From the B-band lightcurve, we estimate a magnitude of $B = 16.3$ mag, while the G400H data yield $B \simeq 16.2$ mag. This is considerably fainter than the $B = 14.7 - 15.5$ mag range previously reported in the literature (Warner & Cropper 1983; Cook & Brunt 1983; Wenzel 1984; Berriman et al. 1986; and Watts et al. 1986). We will thereafter refer to this as the 'low' or 'minimum' brightness state of V2051 Oph to differentiate it from the normal, quiescent state. Thus, our data yield a rare (and lucky) opportunity to cleanly see the white dwarf and bright spot in V2051 Oph, with reduced contributions from the accretion disc and boundary layer to the total light.

Figure 2 shows HST lightcurves at selected passbands, wavelength range increasing upwards. The eclipse shape is reminiscent of those of the dwarf novae OY Car and Z Cha in quiescence (e.g., Wood et al. 1986, 1989), with two compact sources being eclipsed in sequence. Sharp steps corresponding to the egress of the white dwarf and bright spot are clearly seen in the G400H lightcurves. A substantial fraction of the emitted light comes from the white dwarf, which contributes $\simeq 60$ per cent of the total light at 3900-4300 Å. The G160L order zero lightcurve shows the sequence of ingress of two compact sources. The phases of ingress of the first eclipsed source are coincident with those of the white dwarf as estimated from the ground-based data (Fig 3). Hence, we can unambiguously associate the first compact source with the white dwarf and, therefore, the source which is eclipsed later is the bright spot. Egress features of both sources can also be easily identified in the order zero lightcurve. The flux

of the bright spot is larger at ingress than at egress. This is consistent with the overall decrease in brightness along the run and is usually understood in terms of anisotropic emission due to the foreshortening of a spot ‘painted’ at the edge of an optically thick accretion disc. White dwarf and bright spot features are less well defined in the other, lower signal-to-noise ratio G160L lightcurves. Flickering activity – usually higher in the ultraviolet than at optical wavelengths in CVs – is considerably less impressive than observed in quiescence (e.g. Warner & O’Donoghue 1987), probably reflecting the lower brightness state of the system at the epoch of our observations.

The HST dataset gives a clear and simultaneous measurement of the white dwarf and bright spot eclipse phases, which will allow us to estimate the binary mass ratio in section 3.

Figure 3 display the ground-based observations. These lightcurves clearly show the total eclipse of a compact source at disc centre, the white dwarf, and reveal that the white dwarf contributes 80–90 per cent of the light at that epoch, with very little evidence of an accretion disc or bright spot. Flickering activity is mostly suppressed, which is possibly an indication that mass transfer was substantially reduced at that epoch. The duration of the ingress/egress feature ($\simeq 30$ s or 0.006 cycles, see section 3) is shorter than that in quiescence (Warner & Cropper 1983; Berriman et al. 1986; Watts et al. 1986) by a factor of two, possibly an indication that, at those epochs, one was seeing a bright (and larger) boundary layer around the white dwarf instead of the white dwarf itself. This possibility was previously mentioned by Warner & Cropper (1983).

The ground-based dataset yields an unambiguous measurement of the total width of the eclipse of the white dwarf as well as of the duration of its ingress/egress feature and will be crucial for our derivation of the binary parameters in section 3.

3 THE BINARY PARAMETERS

In this section we use measurements of the contact phases of the white dwarf and of the bright spot to develop a model for the binary in V2051 Oph based solely on quantities obtained from the photometry.

3.1 Measuring contact phases

The ingress/egress phases of the occultation of the white dwarf (hereafter WD) and of the bright spot (BS) by the secondary star provide information about the geometry of the binary system and the relative sizes of these components (Wood et al. 1986, 1989). The contact phases can be identified as rapid changes in the slope of the lightcurve, visible in the lightcurves shown in Figs. 2 and 3. We follow the notation of Baptista et al. (1989), taking ϕ_{w1}, ϕ_{w2} as those phases during which WD disappears behind the secondary star and ϕ_{w3}, ϕ_{w4} as the phases corresponding to the reappearance of WD from eclipse. We similarly define a set of phases ϕ_{b1-4} for BS.

The contact phases were measured with the aid of a cursor on a graphic display of a median filtered version of the lightcurve. The estimated error for this procedure is

0.0006 cycles. Mid-ingress (egress) phases for WD and BS (ϕ_{wi}, ϕ_{we} and ϕ_{bi}, ϕ_{be}) were computed as the mid point of the ingress (egress) feature and also as the phase at which half of the compact source light is eclipsed.

We also employed the technique described by Wood, Irwin & Pringle (1985) to measure the contact points and to estimate the phases of mid-ingress (egress), here defined as the points of minimum (maximum) derivative in the lightcurve. Figure 4 illustrates the procedure for the G160L order zero lightcurve. The original lightcurve [Fig. 4(a)] is smoothed with a median filter of width 0.0019 cycles (3 data points) [Fig. 4(b)] and its numerical derivative is calculated. The amount of filtering used at this point is a compromise between the aim to suppress noise in the lightcurve as much as possible and the need to preserve any real structures in the eclipse shape. The ingress/egress of WD and BS can be seen as those intervals for which the derivative curve is significantly different from zero. The width at half-peak intensity of these features yields a preliminary estimate of their duration. A spline function is fitted to the remaining regions in the derivative curve to remove the contribution from the extended and slowly varying eclipse of the disc. The spline-subtracted derivative curve [Fig. 4(c)] is then analyzed by an algorithm which identifies the points of extrema (the mid-ingress / egress phases) and the points where the derivative starts to depart from the zero-constant level (the contact points). A median filter of equal width to that used in the first part of the reduction is applied to the derivative curve to aid in the detection. A similar sequence is used to measure the contact points and mid phases of BS.

Table 3 collects the measured contact phases, mid-ingress and mid-egress phases of WD. Quoted values are the average of the determinations from all methods described above. Uncertain measurements are marked by a colon. Fig. 5 depicts the median contact phases of WD listed in Table 3 in an enlarged view of the combined W+B lightcurve and its derivative curve.

Integrating the flux in the derivative curve Fig. 4(c) between the first and second (third and fourth) contact phases we obtain estimates of the WD flux at ingress (egress). The lightcurve of the WD is then reconstructed by assuming that the flux is zero between ingress and egress and that it is constant outside eclipse. The reconstructed WD lightcurve can be seen in Fig. 4(d), and the lightcurve after removal of the WD component is shown in Fig. 4(e).

For the HST order zero lightcurve (fig. 4), the estimated WD flux at ingress is 0.40 ± 0.05 mJy, larger than the flux of 0.30 ± 0.05 mJy obtained from the egress feature. This could be due to a phase dependent absorption of the WD light, the absorption being more pronounced at egress phases. The analysis of Catalán et al. (1998) suggests that the WD in V2051 Oph is veiled by a large number of blended Fe II lines (the so called Fe II curtain). This effect is reminiscent of that observed previously in OY Car (Horne et al. 1994) and has been attributed to absorption by circumstellar material, possibly in the outer disc. The observed difference in WD flux at ingress and at egress could be associated with this effect if the absorption by the Fe II curtain is more pronounced along the line of sight at egress phases. This seems to be the case in the novalike UX UMa, whose ultraviolet eclipse mapping reveals that the absorption by the Fe II curtain in the disc side closest to the secondary star is more pronounced in the

Table 3. Contact phases of the white dwarf.

run	spectral range	ϕ_{w1}	ϕ_{w2}	ϕ_{w3}	ϕ_{w4}	ϕ_{wi}	ϕ_{we}
H1	3236-3600 Å	–	–	+0.0312	+0.0369	–	+0.0339
	3900-4300 Å	–	–	+0.0303	+0.0365	–	+0.0335
	4400-4781 Å	–	–	+0.0309	+0.0363	–	+0.0337
	3236-4781 Å	–	–	+0.0306	+0.0361	–	+0.0337
H2	1400-1800 Å	–0.0348	–0.0317:	+0.0285	+0.0347	–0.0332	+0.0331
	1802-2303 Å	–0.0361	–0.0298	+0.0279	+0.0361	–0.0330	+0.0325
	1152-2506 Å	–0.0359	–0.0303	+0.0280	+0.0341	–0.0328	+0.0334
	order zero	–0.0366	–0.0309	+0.0305	+0.0355	–0.0334	+0.0330
L1	B	–0.0374	–0.0309	+0.0307	+0.0367	–0.0332	+0.0332
L2	W	–0.0359	–0.0285	+0.0308	+0.0369	–0.0322	+0.0336
L3	W	–0.0356	–0.0300	+0.0302	+0.0367	–0.0333	+0.0334
L4	W	–0.0354	–0.0303	+0.0304	+0.0369	–0.0328	+0.0332
combined W+B		–0.0355	–0.0298	+0.0306	+0.0372	–0.0328	+0.0334
median		–0.0359	–0.0301	+0.0304	+0.0364	–0.0330	+0.0334
error		± 0.0004	± 0.0005	± 0.0003	± 0.0003	± 0.0002	± 0.0002

leading quadrant than in the trailing quadrant (which contains the bright spot and gas stream) and that this effect is probably responsible for a substantial reduction in flux level from before to after eclipse (Baptista et al. 1998b).

Measured BS contact phases, mid-ingress and mid-egress phases are listed in Table 4. As before, quoted values are the average of the determinations from all methods described above. For run H2, only values for the order zero lightcurve are listed since the lightcurves at the other passbands (Fig. 2) do not yield reliable measurements of BS phases. The ingress phases ϕ_{b1} , ϕ_{b2} and ϕ_{bi} were measured from the WD subtracted lightcurve (Fig. 4(e)), which provides an unblended, clean view of the BS ingress feature. The short run H1 gives only the egress phase of the BS, which occurs perceptibly earlier than at run H2. Warner & Cropper (1983) and Warner & O’Donoghue (1987) have shown that the eclipse shape of V2051 Oph (and therefore its disc structure) is very variable and that significant changes occur on the timescale of one orbit. One expects that similar changes in disc radius and BS position do occur in the same timescale. We have thus been cautious not to combine egress phases from different cycles and, therefore, for our procedure to determine the mass ratio q (section 3.2) we will use only the pair of mid-ingress/egress phases of BS measured from run H2. The measurements of mid-ingress/egress phases from the three different methods have dispersions of 0.0005 cycles. However, since only one light curve was used to estimate these values, we adopted more conservative error bars of 0.001 cycles for the mid-ingress phase and 0.002 cycles for the mid-egress phase.

The duration of the WD eclipse is defined as

$$\Delta\phi = \phi_{we} - \phi_{wi}, \quad (2)$$

and the centre of the WD eclipse (the inferior conjunction of the binary) is written as

$$\phi_0 = 1/2 (\phi_{we} + \phi_{wi}). \quad (3)$$

These quantities are collected in Table 5. The median of the measurements from all lightcurves yields $\Delta\phi = 0.0662 \pm 0.0002$ cycles, where the quoted error is the median of the absolute deviations with respect to the median. Similarly, we have $\phi_0 = +0.0000 \pm 0.0002$ cycles, which indicates that the centre of the WD eclipse corresponds to phase zero.

The difference between the first and second (third and fourth) WD contact phases yield the phase width of the WD ingress (egress), Δ_{wi} (Δ_{we}). These quantities are also listed in Table 5. A median from all values of Δ_{wi} and Δ_{we} yields $\Delta_{wd} = 0.0060 \pm 0.0005$ cycles, where again the error is the median of the absolute deviations with respect to the median.

3.2 Mass ratio, inclination and disc radius

Making the usual assumption that the secondary star fills its Roche lobe and given the duration of the eclipse of the central parts of the disc, $\Delta\phi$, there is a unique relation between the mass ratio $q = M_2/M_1$ and the binary inclination i (Bailey 1979; Horne 1985). From Table 5, the width of the eclipse in V2051 Oph is $\Delta\phi = 0.0662$. This gives the constraint $q > 0.116$, with $q = 0.116$ if $i = 90^\circ$.

When combined with the measured contact phases of the WD and BS, this relation gives a unique solution for q , i , and R_{bs}/R_{L1} , where R_{bs} is the distance from disc centre to the BS (usually taken to be the disc radius) and R_{L1} is the distance from disc centre to the inner lagrangian point L1. The following assumptions are made: (i) the infalling gas stream leaving the L1 point describes a ballistic trajectory in the primary lobe (Lubow & Shu 1975), and (ii) the bright spot is located at the position at which the stream hits the edge of the disc. The theoretical trajectories described by a test particle in the primary lobe are solely determined by the mass ratio of the binary. For increasing q values the trajectories are closer to the line joining both stars, as the angular momentum of the infalling gas stream after leaving the L1 point is progressively smaller. The correct mass ratio, and hence inclination, are those for which the calculated stream trajectory passes through the observed position of the bright spot. This method was first developed by Smak (1971) and has since then been applied to various CVs (e.g., Fabian et al. 1978; Cook & Warner 1984; Wood et al. 1986, 1989; Baptista, Steiner & Cieslinski 1994).

Figure 6 illustrates the determination of q , i and R_{bs}/R_{L1} from the eclipse phases. Fig. 6(a) shows a diagram of ingress versus egress phases for the measurements of the WD and BS in Tables 3 and 4. Measurements of the WD ingress and egress are shown as the cluster of small crosses

Table 4. Contact phases of the bright spot.

run	spectral range	ϕ_{b1}	ϕ_{b2}	ϕ_{b3}	ϕ_{b4}	ϕ_{bi}	ϕ_{be}
H1	3236-3600	–	–	+0.0811	+0.0855	–	+0.0831
	3900-4300	–	–	+0.0804	+0.0848	–	+0.0822
	4400-4781	–	–	+0.0811	+0.0836	–	+0.0825
	3236-4781	–	–	+0.0809	+0.0831	–	+0.0821
H2	order zero	−0.0295	−0.0226	+0.0841	+0.0892	−0.0260	+0.0866

Table 5. White dwarf eclipse parameters.

run	spectral range	$\Delta\phi$	ϕ_0	Δ_{wi}	Δ_{we}
H1	3236-3600				0.0057
	3900-4300				0.0062
	4400-4781				0.0054
	3236-4781				0.0056
H2	1400-1800	0.0663	−0.0001	0.0032:	0.0062
	1802-2303	0.0655	−0.0003	0.0063	0.0082
	901-2506	0.0662	+0.0003	0.0056	0.0061
	order zero	0.0664	−0.0002	0.0057	0.0050
L1	B	0.0664	+0.0000	0.0065	0.0060
L2	W	0.0658	+0.0007	0.0074	0.0061
L3	W	0.0667	+0.0000	0.0056	0.0065
L4	W	0.0660	+0.0002	0.0051	0.0065
combined W+B		0.0662	+0.0003	0.0057	0.0066
median		0.0662	+0.0000	0.0057	0.0061
error		±0.0002	±0.0002	±0.0006	±0.0007

around phases (−0.033, +0.033) in the lower portion of the diagram. The small box in the upper left corner marks the $1-\sigma$ range of the mid-ingress and mid-egress phases of the BS. Theoretical gas stream trajectories corresponding to a set of pairs (i, q) are also shown. The trajectories were computed by solving the equations of motion in a coordinate system synchronously rotating with the binary, using a 4th order Runge-Kutta algorithm (Press et al. 1986) and conserving the Jacobi integral constant to one part in 10^6 .

The theoretical trajectory that passes through the position of the BS has $q = 0.19 \pm 0.03$ and $i = 83^\circ 3 \pm 1^\circ 4$, where the uncertainties are taken from the standard deviation of the points about the trajectory of best fit. Fig. 6(b) shows the geometry of the binary system for $q = 0.19$. For this mass ratio, the relative size of the primary Roche lobe is $R_{L1}/a = 0.66$, where a is the orbital separation.

The squashed circle in Fig. 6(a) represents the accretion disc whose edge passes through the position of BS for the adopted mass ratio. This corresponds to a disc radius of $R_{bs}/R_{L1} = (0.56 \pm 0.02)$. A circle with this radius is depicted in Fig. 6(b). The calculated radius is half way between the radius expected for zero-viscosity discs, $R_d/R_{L1} = 0.27$ (Flannery 1975), and that expected for pressureless discs, $R_d/R_{L1} = 0.76$ (Paczynski 1977).

3.3 Masses and radii of the component stars

The duration of the ingress / egress of WD yields an estimate of the relative size of the white dwarf. This information can be used together with the calculated mass ratio to constraint the masses and radii of the component stars. We use the approximate relations of Ritter (1980),

$$2\pi\Delta_{wd} \simeq 2 R_1/[z(q) a \sin \theta], \quad (4)$$

and

$$\cos \theta = \frac{a}{R_2} \cos i, \quad (5)$$

where R_1 and R_2 are the radii of the WD and of the secondary star, and $z(q)$ is the relative distance from disc centre to the point tangent to the surface of the secondary that marks the beginning/end of the eclipse of WD (Baptista et al. 1989). The value of $z(q)$ is a by-product of the inclination-determination routine (section 3.2) and is usually close to unity. In our case, for $q = 0.19$ we have $z = 0.96$. The error introduced by the use of these expressions is of order of $(R_1/R_2)^2$ and for the parameters listed in Table 3 is smaller than 0.5 per cent.

Combining Eq. (4) with Kepler's third law we can write an expression relating the mass and the radius of the white dwarf for V2051 Oph,

$$R_1/R_\odot = 2.349 \Delta_{wd} (M_1/M_{ch})^{1/3} f(q), \quad (6)$$

where $M_{ch} = 1.44 M_\odot$ is the Chandrasekhar mass limit and $f(q) = z \sin \theta (1 + q)^{1/3}$. Another relation between R_1 and M_1 can be obtained from Nauenberg's (1972) analytical approximation to the mass-radius relation for cool degenerate white dwarfs of Hamada & Salpeter (1961),

$$R_1/R_\odot = 0.0112 \left[\left(\frac{M_1}{M_{ch}} \right)^{-2/3} - \left(\frac{M_1}{M_{ch}} \right)^{2/3} \right]^{1/2}. \quad (7)$$

Combining Eqs. (6) and (7) one can solve for $M_1(q, \Delta_{wd})$ and the remaining system parameters.

The primary-secondary mass diagram for V2051 Oph can be seen in Fig. 7. A Monte Carlo propagation code was used to estimate the errors in the calculated parameters. The values of the input parameters q and Δ_{wd} are independently varied according to Gaussian distributions with

Table 6. The calculated parameters of V2051 Oph.

q	0.19 ± 0.03	a/R_{\odot}	0.64 ± 0.02
i	$83.3^{\circ} \pm 1.4^{\circ}$	R_{L1}/a	0.66 ± 0.01
M_1/M_{\odot}	0.78 ± 0.06	R_{bs}/R_{L1}	0.56 ± 0.02
R_1/R_{\odot}	0.0103 ± 0.0007	α_{bs}	$19^{\circ} \pm 1^{\circ}$
M_2/M_{\odot}	0.15 ± 0.03	K_1 (km/s)	83 ± 12
R_2/R_{\odot}	0.16 ± 0.01	K_2 (km/s)	436 ± 11

standard deviation equal to the corresponding uncertainties. The results, together with their $1\text{-}\sigma$ errors, are listed in Table 6. The cloud of points in Fig. 7 was obtained from a set of 10^4 trials using this code. The highest concentration of points indicates the region of most probable solutions.

4 DISCUSSION

4.1 The reliability of the photometric model

Our photometric model is based on the inferred Δ_{wd} and q values. Here we discuss systematic errors which may affect these quantities and their influence on the derived parameters of V2051 Oph, and compare the derived parameters with those obtained by other authors.

Errors in q are related to errors in measuring mid-ingress/egress phases, in particular the BS phases. WD eclipse phases were precisely measured in the ground-based lightcurves, where the BS and the accretion disc give negligible contribution to the total light. These phases helped us to identify the WD eclipse features in run H2 without ambiguities. The lightcurve after the subtraction of the WD contribution (fig. 4(d)) clearly shows the asymmetric eclipse of the compact BS and yielded accurate measurements of its mid-ingress/egress phases. The measured BS phases map into a small region in the ingress/egress phases diagram from which a precise value of q was obtained. Therefore, the mass ratio seems well constrained.

The remaining binary parameters were derived under the assumption that the duration of the ingress/egress of the central object, Δ_{wd} , gives a direct measure of the radius of the white dwarf. This supposition may not always be correct.

It may be possible that the observed compact object of Fig. 5 is a hot and opaque boundary layer involving the white dwarf, in which case the true white dwarf would be smaller than assumed (Wood & Crawford 1986). In this case, the primary mass found is a lower limit. However, notice that increasing the white dwarf mass along the line $q = 0.19$ in Fig 7 results in a secondary star which is overmassive in comparison to a main sequence star of same radius. This would be in marked contrast with the other short-period eclipsing CVs, where the results seem to point in the opposite direction, i.e., secondary stars which are undermassive in comparison to main sequence stars of same radius (Wood et al. 1986, 1989; Horne, Wood & Stiening 1991). Other effects that may result in an overestimated white dwarf radius include the questionable application of a mass-radius relation for cool white dwarfs to a relatively hot object (Horne, Wood & Stiening 1991), and a possible spherical distortion for a white dwarf rotating close to breakup velocity (Wood & Horne 1990). However, the corrections in the derived parameters implied by these effects ($\lesssim 5$ per cent) are smaller

than the uncertainty in the value of Δ_{wd} and were not taken into consideration.

Alternatively, could the white dwarf be larger than inferred from our value of Δ_{wd} ? We now address two possibilities in this regard.

Previous eclipse photometry of V2051 Oph indicate a duration of the ingress/egress of the compact central source of $\Delta_{wd} \simeq 0.009 - 0.012$ (Warner & Cropper 1983; Cook & Brunt 1983; Watts et al. 1986), substantially larger than measured from our observations. However, the variability and the clear correlation between brightness and duration of ingress/egress of this source led Warner & Cropper (1983) to suggest that it might be a bright (and variable) boundary layer around the white dwarf and not the white dwarf itself. This scenario is supported by our observations at minimum light, when mass accretion has probably been substantially reduced and the boundary layer has accordingly dimmed, leaving a bare, fainter, and much smaller white dwarf as the only light source at disc centre.

Warner & O'Donoghue (1987) suggested that V2051 Oph could be a low field polar. Following their suggestion, we explored the possibility that the observed compact source at disc centre is in fact a bright spot at the surface of the white dwarf, corresponding to the pole of an accretion column. If the white dwarf rotates synchronously with the binary, one would expect the lightcurves to show a strong orbital modulation due to the self occultation of the accretion column. For example, at phase $\phi = 0.25$ about half of the accretion column would have disappeared behind the white dwarf resulting in a reduction of $\gtrsim 40$ per cent in flux of the lightcurve. On the other hand, if the white dwarf is non synchronously rotating, one would expect to see two conspicuous effects in the lightcurves: (1) large amplitude ($\simeq 40$ per cent) pulsations with the rotation period of the white dwarf, and (2) measurable wanderings of the ingress/egress phases and eclipse width of the compact source at disc centre as the accretion column is seen at different aspects. Our observations clearly exclude both possibilities: there is no sign of strong orbital modulation, no sign of pulsations, and no detected changes in eclipse phases. Therefore, we are left with the conclusion that the compact source at disc centre of our observations is indeed the white dwarf.

It is worth mentioning that our observations do not discard the possibility that V2051 Oph possess a magnetic white dwarf. If the observed minimum brightness state corresponds to a phase of reduced mass transfer and negligible or no mass accretion, then no emission would be produced in the accretion column, which could therefore remain undetected.

We now turn to the comparison of our derived parameters with those obtained by Watts et al. (1986). Their dynamical model of V2051 Oph is based on spectroscopy of the accretion disc's emission lines. Radial velocity for the $H\beta$ and $H\gamma$ lines yields a $K_1 = 111 \text{ km s}^{-1}$ and a phase lag of $+0.13$ cycles with respect to the photometric phase. Phase lags of $0.1 - 0.2$ cycles between photometric and spectroscopic conjunction are seen in many of the CVs for which emission lines radial velocity curves were measured. Asymmetries in the line intensity distribution (which displace the light centroid from disc centre) or the existence of a non-circular component to the velocity of the emitting gas (as it may happen in the presence of a disc wind) lead to sys-

tematic errors in the amplitude and phase of the measured K_1 . They show that the observed phase lag of V2051 Oph can be explained if the accretion disc is asymmetric in the emission lines, with the trailing lobe being $\simeq 60$ per cent brighter than the leading lobe. The measured K_1 will be overestimated by $\simeq 22$ per cent in this case. The correction of their K_1 value by this effect eliminates the phase lag and brings their measurement to $K_1 = 91 \text{ km s}^{-1}$, into good accordance to our prediction in Table 3.

Watts et al. (1986) used the double peaked Balmer line profiles and their behaviour during eclipse to constrain the mass ratio of the binary. Their model predicts a larger mass ratio ($q = 0.26 \pm 0.04$) and a much smaller white dwarf mass ($M_1 = 0.43 \pm 0.05 M_\odot$) than ours. We note that their fit to the line behaviour during eclipse seems of rather poor quality. The larger spectroscopic mass ratio predicts that the bright spot eclipse occurs earlier than observed, with a phase difference at the $2\text{-}\sigma$ level. The spectroscopic model also predicts a duration of the ingress and egress of the white dwarf of $\Delta_{wd} = 0.011$, which clearly conflicts with the observed duration of $\Delta_{wd} = 0.0060 \pm 0.0005$.

It would be useful to have another observational constraint on the binary parameters. The best way of checking the reliability of the above assumptions in calculating binary parameters is to measure the radial velocity of the secondary star, K_2 .

4.2 The low brightness state: reduced mass transfer rate?

At the time of our observations V2051 Oph was in a much lower brightness state than at quiescence, when it has $V \simeq 15$ mag. Since it was observed to be in this lower brightness state both in 1996 January and in 1996 June, it may be possible that this is a relatively prolonged minimum state of duration a few months. Recovery of photometric observations of V2051 Oph during this period would be important to clarify this point.

The system has been observed to go into outburst once, where it increased in brightness to reach $V \simeq 13.2$ (Warner & O'Donoghue 1987). If the outburst is caused by the disc instability mechanism, than the disc is *already* in a state of low viscosity, low mass accretion rate when the system is at $V \simeq 15$ mag. Therefore, it is hard to explain the observed low brightness state in terms of disc instability. The simplest way to understand the reduced brightness level of V2051 Oph is to consider it the consequence of a significant reduction in the mass transfer rate.

4.3 The secondary star mass and its evolutionary consequences

Our photometric model indicates that V2051 Oph has a larger mass ratio and a more massive white dwarf than the other eclipsing dwarf novae of similar period. Probably more relevant, it has a secondary star which is significantly more massive than those of Z Cha, OY Car and HT Cas. Since the inferred size of the secondary in these systems is similar, $R_2/R_\odot \simeq 0.15$, this means that the secondary star of V2051 oph is much denser than those of the other dwarf novae.

Theoretical evolutionary models of CVs predict that the long term, continuous mass loss brings the secondary stars out of thermal equilibrium and make these stars larger than a main sequence star of same mass (Rappaport, Joss & Webbink 1982). Hence, the fact that the secondary stars in Z Cha, OY Car and HT Cas are oversized in comparison to main sequence stars of same mass suggests that these systems are relatively old cataclysmic variables, for which mass transfer (and loss from the secondary) has been occurring for some 10^9 years. On the other hand, the fact that the secondary star of V2051 Oph obeys a typical main sequence mass-radius relationship suggests that V2051 Oph is a relatively young system, for which mass loss has not occurred for long enough time to bring the secondary star out of thermal equilibrium. Further support to this suggestion comes from the following argument. If we assume that CVs evolve by losing mass in recurrent nova outbursts (at a rate of $\simeq 10^{-5} M_\odot$ at every $10^4 - 10^5$ years), than V2051 Oph will need about 10^9 years to reduce its total mass of about $0.9 M_\odot$ to the typical total mass of $\simeq 0.7 M_\odot$ of the other, older dwarf novae of similar orbital period.

For a star out of thermal equilibrium, the ability to shrink in response to mass loss is substantially reduced and one expects this star to loose mass at a higher rate than a star of same mass but still in thermal equilibrium. If the young secondary star in V2051 Oph is still in thermal equilibrium, then it may have a smaller rate of mass loss than the secondary stars of evolved CVs of similar orbital period. Hence, it may be possible that V2051 Oph has a considerably smaller mass transfer rate than that of Z Cha, OY Car and HT Cas. According to the disc instability model, the time interval between outburst can be substantially increased if the mass transfer rate is significantly reduced. This could be an explanation of why the outbursts in V2051 Oph are so rare (only one has been reported in 20 years of observations).

5 CONCLUSIONS

The analysis of HST/FOS and ground-based eclipse observations of the dwarf novae V2051 Oph yielded the following results:

(i) V2051 Oph was observed in a low brightness state, at $B \simeq 16.2$ mag. In comparison to the average IUE spectra, the ultraviolet continuum and emission lines appear reduced by factors of, respectively, $\simeq 4$ and $\simeq 5$. Flickering activity is mostly suppressed and the lightcurve shows the eclipse of a compact white dwarf at disc centre which contributes $\simeq 60$ per cent of the total light at $3900\text{--}4300 \text{ \AA}$. In 1996 January, the bright spot is clearly seen in the lightcurve, allowing a precise measurement of its eclipse phases. In 1996 June only the white dwarf is seen in the lightcurve and its radius can be estimated from accurate measurement of the width of its ingress/egress. It is suggested that this state is the consequence of a substantial reduction in mass transfer rate.

(ii) We developed a purely photometric model for the binary from the eclipse phases of the white dwarf and bright spot. For the gas stream trajectory to pass through the position of the bright spot a mass ratio $q = 0.19 \pm 0.03$ is required. The corresponding inclination is $i = 83^\circ.3 \pm 1^\circ.4$.

(iii) The duration of the ingress/egress of the white dwarf combined with the Hamada-Salpeter mass-radius relationship and the obtained mass ratio give $M_1 = 0.78 \pm 0.06 M_\odot$ and $M_2 = 0.15 \pm 0.03 M_\odot$. Calculated parameters are summarized in Table 6.

(iv) The secondary of V2051 Oph is significantly more massive than the secondaries of the other ultra-short period dwarf novae and seems to obey a ZAMS mass-radius relationship. V2051 Oph is probably a relatively young system, whose secondary star had not enough time to evolve out of thermal equilibrium. It is also suggested that V2051 Oph has a lower mass transfer rate than the other ultra-short period dwarf nova. This would explain why outbursts in V2051 Oph are so rare (only one has been observed in a timescale of 20 years).

(v) Our photometric model predicts $K_1 = 83 \pm 12 \text{ km s}^{-1}$, which is in accordance with the velocity amplitude obtained from the emission lines after a correction for asymmetric line emission in the disc is made (Watts et al. 1986).

ACKNOWLEDGMENTS

We thank an anonymous referee for valuable comments and suggestions on an earlier version of the manuscript. RB acknowledges financial support from CNPq/Brazil through grant no. 300 354/96-7.

REFERENCES

- Bailey J., 1979, MNRAS, 187, 645
 Baptista R., Jablonski F.J., Steiner J.E., 1989, MNRAS, 241, 631
 Baptista R., Steiner J. E., Cieslinski D., 1994, ApJ, 433, 332
 Baptista R., Triplet L., Bond H., 1998a, PASP, in preparation
 Baptista R., Horne K., Wade R., Hubeny I., Long K., Rutten R.G.M., 1998b, MNRAS, in press
 Berriman G., Kenyon S., Bailey J., 1986, MNRAS, 222, 871
 Bond H., Wagner R.L., 1977, IAU Circular 3049
 Bruch A., 1983, IBVS, 2287
 Catalán M.S., Horne K., Cheng F.-H., Marsh T., Hubeny I., 1998, preprint
 Cook M.C., Brunt C.C., 1983, MNRAS, 205, 465
 Cook M.C., Warner B., 1984, MNRAS, 207, 705
 Eracleous M., Horne K., 1994, ApJ, 433, 313
 Fabian A.C., Lin D.N.C., Papaloizou J., Pringle J.E., Whelan J.A.J., 1978, MNRAS, 184, 835
 Flannery B.P., 1975, MNRAS, 170, 325
 Hamada T., Salpeter E.E., 1961, ApJ, 134, 683
 Horne K., 1985, MNRAS, 213, 129
 Horne K., Marsh T.R., Cheng F.-H., Hubeny I., Lanz T., 1994, ApJ, 426, 294
 Horne K., Wood J.H., Stiening R.F., 1991, ApJ, 378, 271
 Graham J.A., 1982, PASP, 94, 244
 Jablonski F.J., Baptista R., Barroso Jr. J., Gneiding C., Rodrigues F., Campos R.P., 1994, PASP, 106, 1172
 Lamla E., 1981, Landolt-Börnstein - Numerical Data and Functional Relationships in Science and Technology, Vol. 2, eds. K. Schaifers & H.H. Voigt, Springer-Verlag
 Lubow S.H., Shu F.H., 1975, ApJ, 198, 383
 Nauenberg M., 1972, ApJ, 175, 417
 Paczyński B., 1977, ApJ, 216, 822
 Press W.H., Flannery B.P., Teukolsky S.A., Vetterling W.T., 1986, Numerical Recipes, Cambridge University Press
 Pringle J. E., Verbunt F., Wade R. A., 1986, MNRAS, 221, 169
 Rappaport S., Joss P.C., Webbink R.F., 1982, ApJ, 254, 616
 Robinson E.R., 1992, Viña del Mar Workshop on Cataclysmic Variable Stars, ASP Conference Series Vol. 29, Ed. N. Vogt, Astron. Soc. Pac., San Francisco, p.3
 Ritter H., 1980, A&A, 86, 204
 Sanduleak N., 1972, IBVS, 663
 Smak J., 1971, Acta Astr., 21, 15
 Stone R.P.S., Baldwin J.A., 1983, MNRAS, 204, 347
 Vogt N., 1983, A&AS, 53, 21
 Warner B., 1996, Cataclysmic Variable Stars, Cambridge Astrophysics Series 28, Cambridge University Press
 Warner B., Cropper M., 1983, MNRAS, 203, 909
 Warner B., O'Donoghue D., 1987, MNRAS, 224, 733
 Watts D.J., Bailey J., Hill P.W., Greenhill J.G., McCowage C., Carty T., 1986, A&A, 154, 197
 Wenzel, W., 1984, IBVS, 2481
 Wood J.H., Crawford C.S., 1986, MNRAS, 222, 645
 Wood J.H., Horne K., Berriman G., Wade R., O'Donoghue D., Warner B., 1986, MNRAS, 219, 629
 Wood J.H., Horne K., Berriman G., Wade R., 1989, ApJ, 341, 974
 Wood J.H., Horne K., 1990, MNRAS, 242, 609
 Wood J.H., Irwin M.J., Pringle J.E., 1985, MNRAS, 214, 475

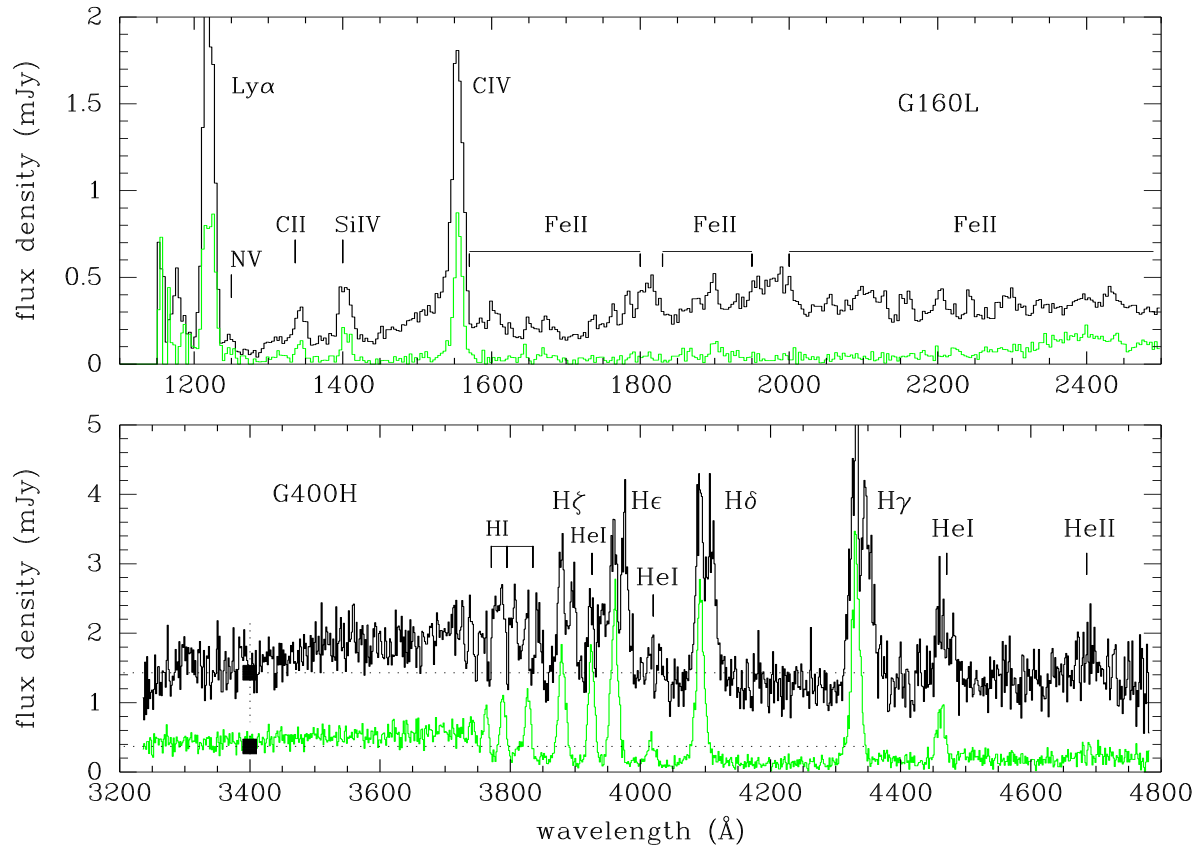


Figure 1. Average out-of-eclipse (black) and mid-eclipse (light gray) HST spectra of V2051 Oph. Major emission and absorption features are labelled. Phase ranges of each spectrum are as follows: +0.1 to +0.3 (G160L, out of eclipse), -0.02 to +0.03 (G160L, mid-eclipse), +0.082 to +0.09 (G400H, out-of-eclipse), and +0.02 to +0.03 (G400H, mid-eclipse). Filled squares in the G400H panel indicate the fluxes of the G160L order zero light computed at the same phase ranges as the G400H average spectra. Horizontal dotted lines show the FWHM of the G160L order zero passband.

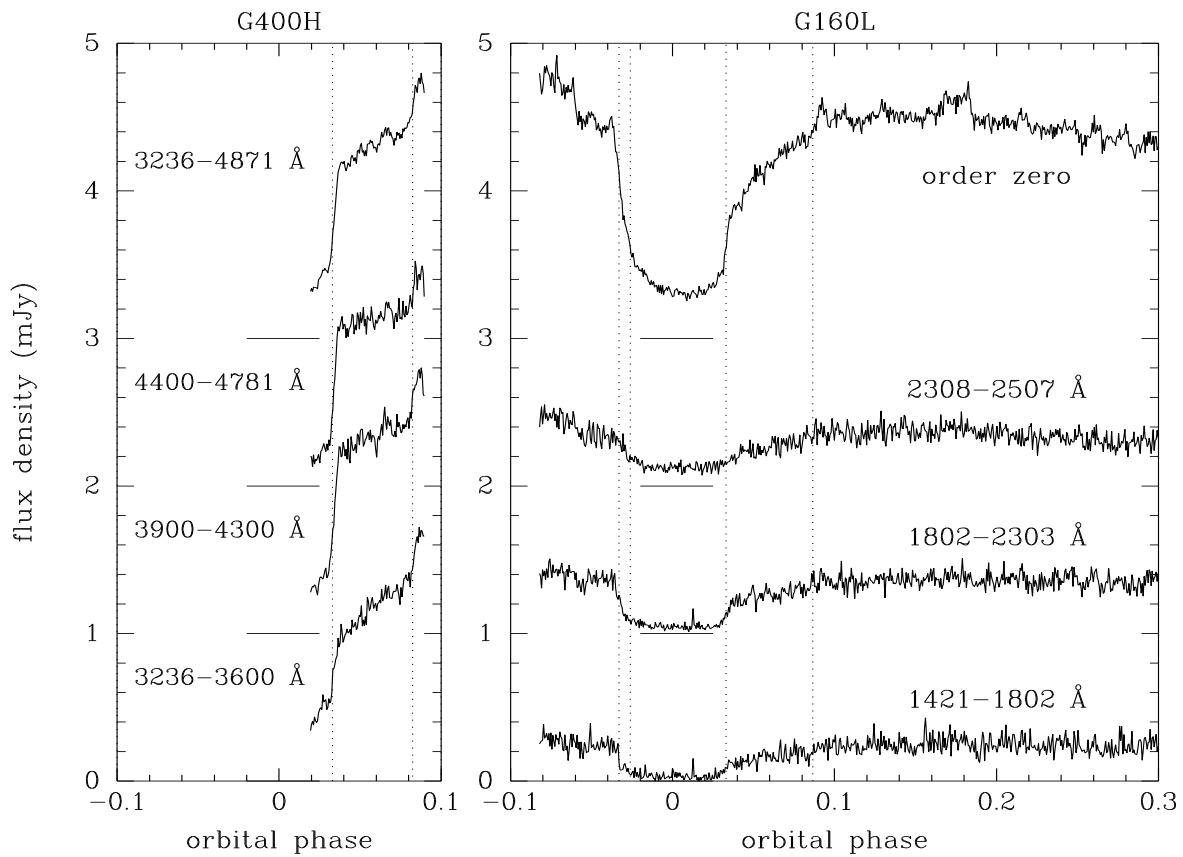


Figure 2. HST lightcurves of V2051 Oph at selected passbands, for the G400H (left) and G160L (right) data. The 1421-1802 Å lightcurves excludes the region of the CIV $\lambda 1550$ doublet. The curves are progressively displaced upwards by 1 mJy. Horizontal lines at mid-eclipse show the true zero level in each case. Vertical dotted lines mark ingress/egress phases of the white dwarf and bright spot as measured in section 3.

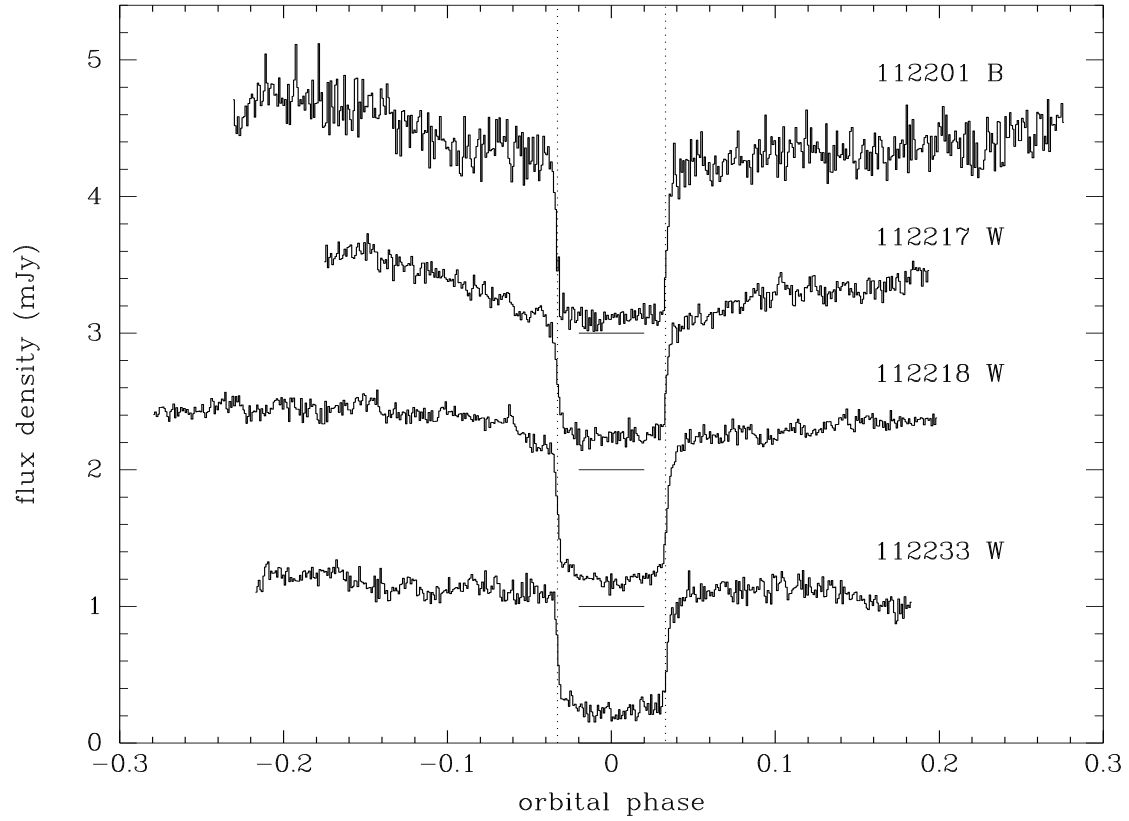


Figure 3. Ground-based lightcurves of V2051 Oph. The white light lightcurves were artificially scaled to the same out-of-eclipse level of the B-band lightcurve for simplicity of display. The curves are progressively displaced upwards by 1 mJy. Horizontal lines at mid-eclipse show the true zero level in each case. Vertical dotted lines mark ingress/egress phases of the white dwarf as measured in section 3.

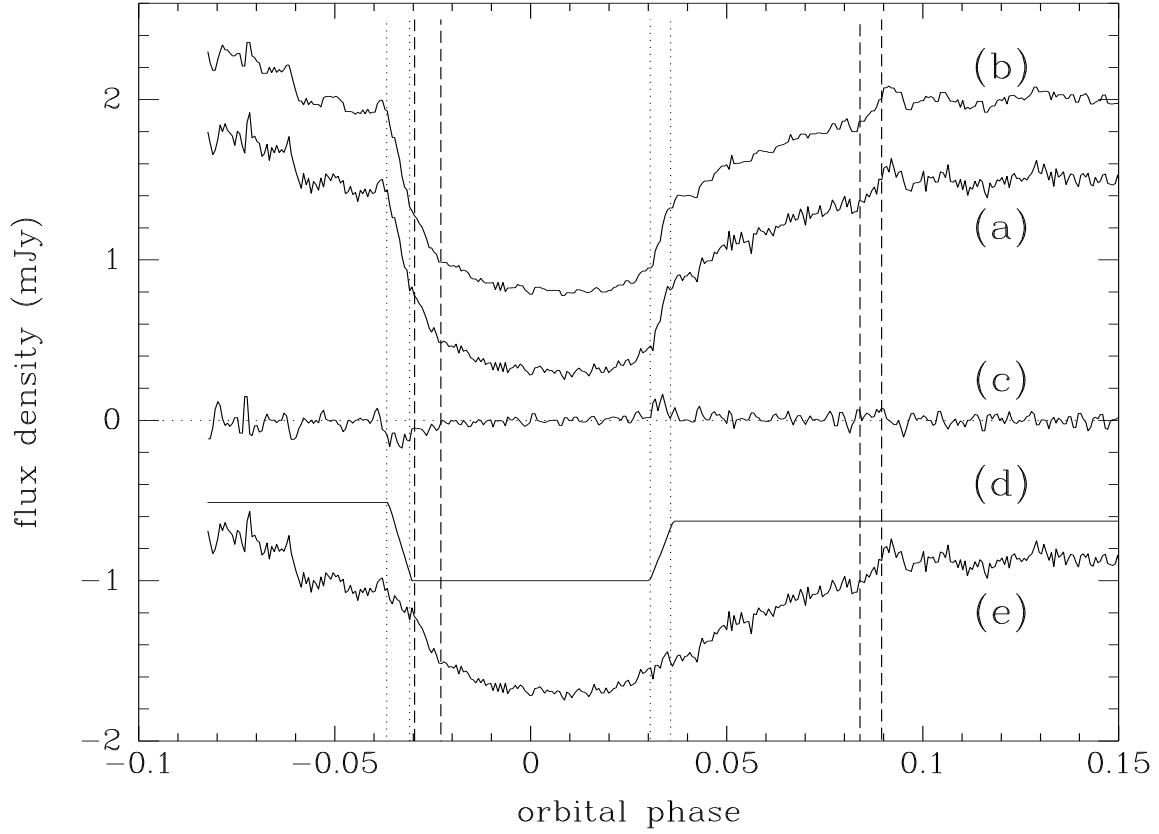


Figure 4. Example of measuring contact phases in a lightcurve of V2051 Oph. (a) Original G160L white light lightcurve at a time resolution of 5×10^{-5} cycles. (b) median-filtered lightcurve, shifted upwards by 0.5 mJy. (c) the derivative of lightcurve (b) after removing the slowly-varying disc component, multiplied by a factor 2. (d) the reconstructed white dwarf lightcurve, shifted downwards by 1 mJy. (e) the lightcurve without the white dwarf component, shifted downwards by 2 mJy. Dotted lines mark the contact phases of the white dwarf and dashed lines mark the contact phases of the bright spot.

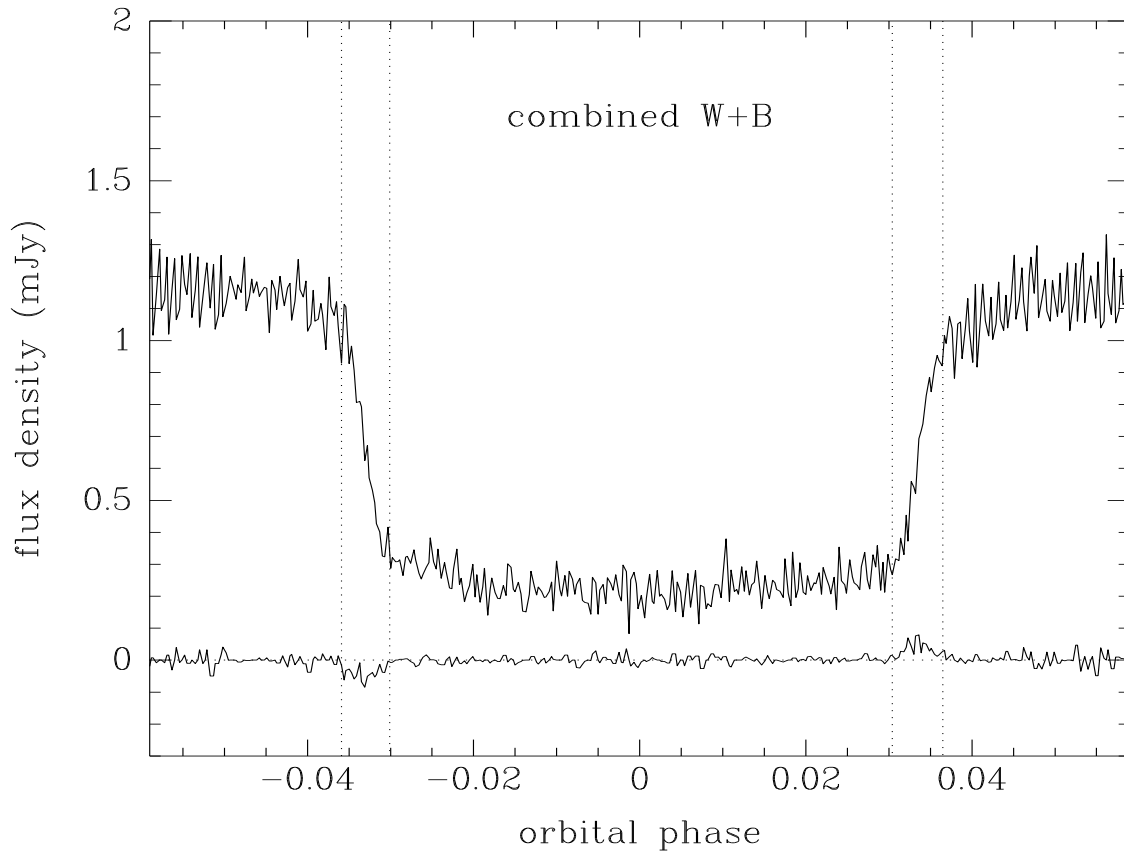


Figure 5. The combined W+B lightcurve (runs L1 to L4) and its derivative curve. Vertical dotted lines depict the median contact phases of the WD as listed in Table 3.

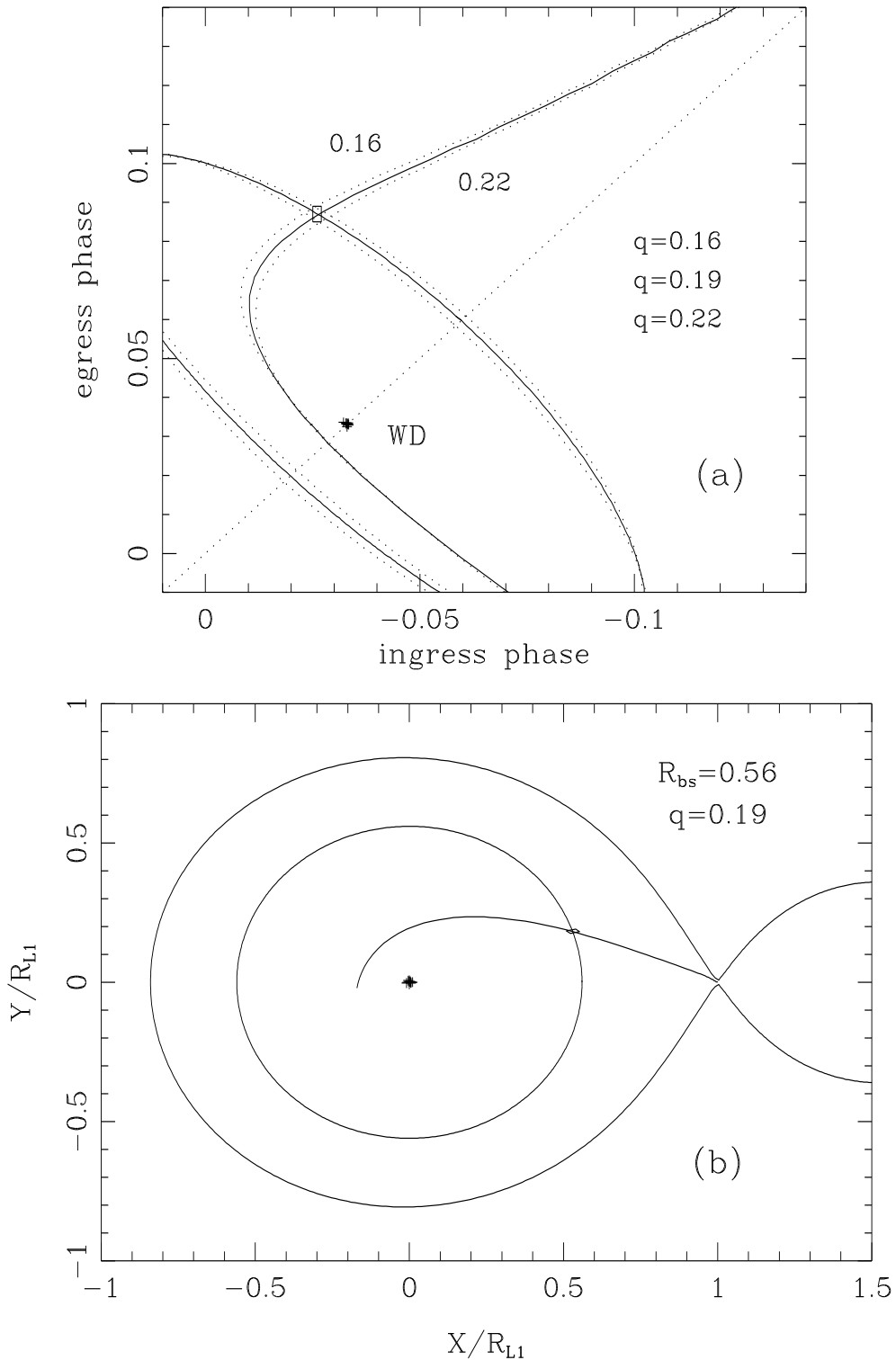


Figure 6. Inferring the binary geometry from the ingress/egress phases of WD and BS. (a) Ingress-egress phases diagram. The observed phases of mid-ingress/egress of WD are marked with crosses, those of BS with a small box. A diagonal dotted line depicts the line joining the component stars. Theoretical gas stream trajectories for various values of q are plotted. The stream of matter passes through the position of BS for $q = 0.19$. The squashed circle represents the accretion disc whose edge passes through the position of BS, for $q = 0.19 \pm 0.03$. This yields a disc radius of $R_{bs} = 0.56 R_{L1}$. (b) the adopted geometry of the binary for $q = 0.19$. The observed positions of WD and BS are shown with the theoretical gas stream and a disc of radius $R_{bs} = 0.56 R_{L1}$.

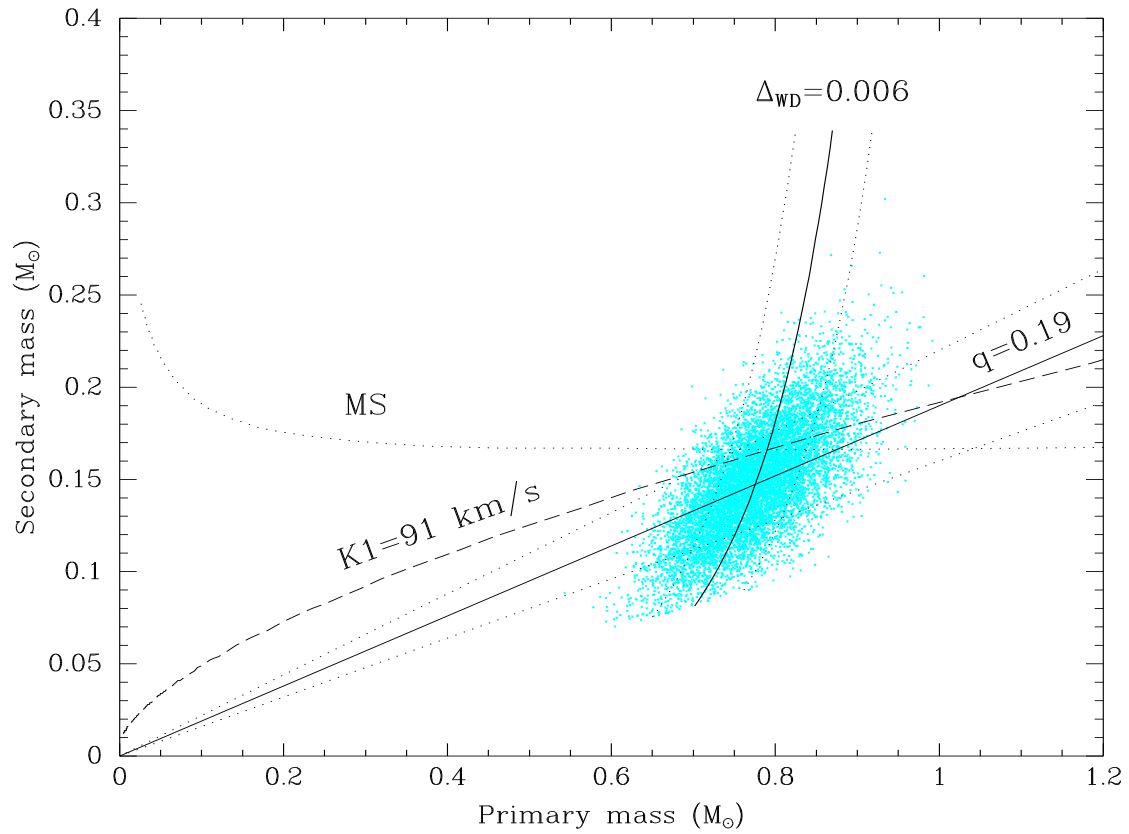


Figure 7. Primary - Secondary mass diagram for V2051 Oph. Solid lines show the constraints obtained from the measured Δ_{wd} and the inferred mass ratio of $q = 0.19$. Dotted lines indicate the $1\text{-}\sigma$ limit on these relations. The mass function for a white dwarf radial velocity of $K_1 = 91 \text{ km/s}$ (Watts et al. 1986) is shown as a dashed line and a mass-radius relation of $R_2/R_\odot = M_2/M_\odot$ is shown as a dotted line. The gray cloud of points shows the confidence region and is the result of a 10^4 points Monte Carlo simulation with the values of Δ_{wd} and q .